Desalination and Water Treatment
www.deswater.com

doi: 10.5004/dwt.2022.28717

267 (2022) 293–303
August

Fabrication of a novel positively charged MIL-101(Al and Cr)-NH_2/polyvinyl alcohol nanofiltration membrane for methylene blue cationic dye separation

Mohsen Mehdipour Ghazi*, Abbas Bagherian

Faculty of Chemical, Petroleum and Gas Engineering, Semnan University, Semnan 35131-19111, Iran, emails: Mohsenmehdipour@semnan.ac.ir (M.M. Ghazi), Abbas.b.68@semnan.ac.ir (A. Bagherian)

Received 21 February 2022; Accepted 11 July 2022

ABSTRACT

This study aimed at investigating the effective removal of cationic dye (methylene blue) and multivalent cation by a novel positively charged nanofiltration composite membrane. This nanofiltration membrane was made by incorporating two types of amino-metal–organic frameworks named MIL-101(Al)-NH_2 and MIL-101(Cr)-NH_2 with a positive charge as fillers into polyvinyl alcohol polymeric matrix. Optimal concentration of the polyvinyl alcohol and filler was evaluated to enhance removal efficiency of particles. Fillers could homogeneously spread in polyvinyl alcohol aqueous solution and form a thin layer above the polysulfone substrate. The effect of metal–organic framework types and their content on the membrane structure were studied by X-ray diffraction, Fourier-transform infrared spectroscopy, field-emission scanning electron microscopy, zeta potential and water contact angle. The filler morphology and its content into polyvinyl alcohol matrix (0%–20%) affected significantly on membrane performance and fouling. MIL-101(Al)-NH_2 had a smaller structure than grainy MIL-101(Cr)-NH_2. The results showed that the membrane filled with MIL-101(Al)-NH_2 achieved higher flux permeability and rejection compared with that of filled with MIL-101(Cr)-NH_2. Although the membrane permeate flux was approximately 15 L/m^2 h with a reasonable fouling and cleaning properties, this MIL-101(Al)-NH_2/polyvinyl alcohol nanofiltration membranes could reject up to 99% of methylene blue because of electrostatic repulsion effect. It is suggested that the fabricated nanofiltration membrane be used to purify dilute amounts of cationic dye

Keywords: Nanofiltration; Electrostatic repulsion; MIL-101(Cr)-NH_2; MIL-101(Al)-NH_2; Polyvinyl alcohol; Methylene blue

1. Introduction

Dyes are used as coloring agents in different industries (e.g., leather, textiles, food, cosmetics, pharmaceuticals, and so on). These dyes are the pollutants that discharged into nature through the sewage system. The main concern regarding the dyes is toxicity and environmental disturbances [1–3]. Positively charged dyes, have been used widely among industrial dyes in printing and dyeing cotton and textiles; for example, methylene blue (MB) and rhodamine B (RhB) [4–6]. The MB concentration, usually ranges from 10–200 ppm in wastewater discharged into the environment, and is highly harmful for the environment and human health [7–9]. In recent decades, substantial research has been conducted to improve materials progressively [10,11] and technological devices [12] increased freshwater supply by wastewater reuse or seawater as well as brackish water desalination. Amid the recent research, membrane filtration has high separation yield, low materiel expenditure, and low energy waster [13,14]. In fact, 'the nanofiltration' (NF) membrane has been a suitable water treatment technology to separate multivalent salts

---

* Corresponding author.

1944-3994/1944-3986

and organic molecules [15] in that diffusion, electrostatic repulsion, and size exclusion are the principal mechanisms for solute separation [16]. The development of high permeability and excellent selectivity NF membranes are essential [17]. Advanced 'NF membranes, forming a thin-film composite (TFC) design [18], are made of a skin layer deposited on top of typically porous support, such as ultrafiltration (UF) [19] or microfiltration (MF) membrane [20]. TFC structure leads to high performance and mechanical integrity of the membrane and enables scalable membrane fabrication at a reasonable cost [21]. In the case of polymeric materials, polyamides and aromatic polyamides are ideally known as ultra-thin synthetic coatings. Polyvinyl alcohol (PVA) polymer has excellent physical and 'chemical stability' in organic solvents. It can be attractive in terms of membranes due to permeability of high water and good film-forming properties. Also, this is easily soluble in water without any additional solvents [22]. Thus, PVA can form a selective skin layer in forming thin-film composite membranes for the organic solvent pervaporation [23]. However, when it is used as a reverse osmosis (RO) membrane, is generally lacking in the rejection of salts [24]. PVA molecules are cross-linked together by dialdehydes and dibasic acids as cross-linkers to improve membrane selectivity [25]. In addition, various additives, including nanoparticles such as zeolite [26], silica [27] and titanium dioxide [28], used as fillers to fabricate thin-film nanocomposite (TFN) and 'mixed matrix membranes'. These fillers help to improve membrane performance and characteristics. Over the last decade, many attempts have been made to create a recent kind of 'porous material relies on metal–organic frameworks' (MOFs) known as the hybrid organic-inorganic framework or coordination polymers. Over the last decade, efforts to create a new type of porous material in the base metal–organic framework (MOF) is carried out in the framework of inorganic–organic hybrid materials or polymers are coordinates.

MOFs consist of metal cores forming a structure of texture by 'organic binders' [29]. Currently, these materials are highly regarded because of their unique features (e.g., high pore volume [30] and surface area [30,31], low density [32], numerous adsorption sites, and various structures). These features promote several particular applications [29] in great deal of regions, that is, 'gas storage, separation processes, catalysis and water treatment' [33–36]. Among various applications, separation, filtration and membrane processes were further investigated. Overall, MOF particles can improve the structure and separation performance of membranes in waste water treatment [37]. MOFs in NF membranes have many advantages over other inorganic fillers: they not only have a better tendency to polymer chains to prevent non-selective cavities but may also remove certain particles based on their shape, size, polarity, and structure [38].

MIL-n type MOF (for Materials Institute Lavoisier), first introduced by Férey et al. [39,40], is a porous metal carboxylate with an open framework that was developed using trivalent cations such as chromium(III) and iron(III), aluminium(III), gallium(III) or indium(III). Their topology is similar to some zeolites but has different surface chemistry, density, and pore sizes [39,40]. From MIL-n type MOFs, the MIL-101 series that are primarily used in gas separation membranes [41–44], has a cubic structure that consists of 2.9 and 3.4 nm mesoporous cages containing 1.2 and 1.6 nm microporous windows [45]. MIL-101 is also an ideal candidate as filler for NF mixed matrix membranes due to its high stability in water and conventional solvents [46] and high surface area and porosity [47]. The presence of various functional groups in the MOF primary reactants and or incorporated functional groups by post-synthesis modification of organic ligands and unsaturated metal sites within the framework can regulate the physical and chemical properties of MOFs [48,49]. Amine groups are very diverse and can be placed into many MOF structures by using the amino ligand 2-amino-1,4-benzene dicarboxylate (BDC-NH_2) during MOF synthesis. The amine group on the organic ligand structure helps to develop further functionalized MOFs through post-synthetic modifications. Also it can improve the tendency of specific molecules such as the adsorption of anionic particles or the repulsion of cationic molecules [50]. MIL-101-NH_2 retains the basic structural properties of MIL-101. At the same time, the presence of amine groups creates an additional positive charge in its structure and helps its better dispersion in the PVA polymer matrix [45]. The presence of this MOF in the membrane structure, because of electrostatic repulsion, can be effective in repelling positive particles such as MB dye molecules.

2. Materials and methods

2.1. Materials

Polysulfone pellets from Solvay Polymer were used as substrate membrane polymer. BDC-NH_2 (99%) purchased from Sigma-Aldrich. Polyethylene glycol 400 (PEG400), Triton X-100 (TX-100) and N,N-dimethylformamide (DMF, ≥99.9%) were used as pore former, surfactant and solvent, respectively. These materials were purchased from Merck. Also, sodium dodecyl sulfate (SDS), aluminium chloride hexahydrate ($AlCl_3\cdot6H_2O$, crystallized, ≥99.0%), chromium(III) nitrate nonahydrate ($Cr(NO_3)_3\cdot9H_2O$), acetone, ethanol, methanol (99%), PVA (molecular weight: 72000), glutaraldehyde and sulfuric acid (98%) were taken from Merck and used without more purification. De-ionized water and MB dye as sample feed solution were used through this work.

2.2. MOFs synthesis

In this study, two types of amino MOFs in the MIL family named MIL-101(Al)-NH_2 (NM101A) and MIL-101(Cr)-NH_2 (NM101C) were synthesized and utilized as NF membrane fillers. For the synthesis of NM101A, according to previous reports [43,51], at first 0.51 g of $AlCl_3\cdot6H_2O$ was dissolved in 30 mL of DMF, and then 0.56 g of BDC-NH_2 was added to this solution. Next, the solution containing metal core and ligand was stirred for about 20 min, and the reaction was then completed in a Teflon-lined autoclave at 130°C for 72 h.

Finally, 'the autoclave' was cooled to room temperature, and the product was obtained as a yellow powder after solution centrifugation at 10,000 rpm, several steps of washing with acetone, activation with methanol, and then drying at 100°C for 24 h.

NM101C was synthesized using water solvent and hydrothermal method in which, according to previous works [52], 2.5 g $Cr(NO_3)_3·9H_2O$ and 1.14 g BDC-NH_2 ligand were dissolved in 35 g water for 20 min. After completing the reaction in a Teflon-lined autoclave at 130°C for 24 h, the product was separated by centrifugation and after washing with acetone thoroughly dried and stored.

2.3. Preparation of MOF/PVA NF membranes

An ultra-thin layer of PVA was formed on the polysulfone substrate. The support membrane, which was made by phase change method, had finger holes and a narrow and dense surface. The casting solution contained 16 wt.% polysulfones, 1 wt.% PEG400 and 2 wt.% of TX-100. These materials were dissolved in DMF at ambient temperature for 8 h. After ensuring the solution became bubble free after 10 h, the solution was cast on a nonwoven polyester by a casting knife with a thickness of 160 μm and directly immersed in an aqueous solution bath containing 1 wt.% SDS to complete the phase separation process for 24 h. This polysulfone membrane had a flux of 100 L/m^2 h bar and a contact angle of approximately 74.38° and was saved in pure water prior to using.

For preparing the MOF/PVA NF membranes, polysulfone substrate was first cut to appropriate dimensions, and dried at room temperature. Then this support membrane was fitted between two frames that were sealed by washers and clamps for casting the solutions. The constructive solution of selective layer for coating the substrate surface was a 7 mL aqueous solution of PVA with specific weight percentage (0.6–1 wt.%), which was obtained by dissolving PVA powder in pure water at 90°C for 5 h. A uniform, constant-concentration solution of PVA containing different amounts of MOFs including 0%, 5%, 10%, 15%, and 20% (calculated by Eq. (1)) as filler was obtained by adding MOF powder into the PVA solution step by step, under stirring and then ultrasonic waves. These membranes are listed in Table 1.

$$W\%_{\text{MOF}} = \frac{M_{\text{MOF}}}{M_{\text{PVA}}} \times 100 \tag{1}$$

The coating solution was casted on top of polysulfone porous membrane and dried at 50°C for 3 h. All the dried membranes were cross-linked with 25 mL solution containing 0.15 wt.% glutaraldehyde and 1 wt.% sulfuric acid as a catalyst for 20 min and at temperature of the room. The final membranes were obtained after drying at room temperature.

2.4. Characterization

'X-ray diffraction (XRD; Bruker, D8 Advance) with a scanning pace' of 0.05°/s and 'Fourier-transform infrared spectroscopy' (Shimadzu, Japan FTIR 8400s Spectrometer) in 4,000–400 cm^{-1} wavenumber range at room temperature were used to characterize the crystalline structure and to investigate the molecular structure of MOFs, respectively. The MOFs structure and NF membranes cross-section and surface morphologies were evaluated by field-emission scanning electron microscopy (FESEM) (Model: TESCAN MIRA3 XMU) at 10 kV.

Contact Angle and Interfacial Tension Analyzer (CA-ES10, Fars Overdraft Technology, Iran) measured membrane surface water contact angle using de-ionized water at 25.0°C. Also water contact angle has been used to measure the membrane surface hydrophilicity. An average of different contact angle measurements was taken at different points of the membrane sample.

An electrokinetic analyzer (EKA, Anton Paar GmbH, Austria) was used to measure the surface streaming potential using 0.001 mol/l KCl solution at 25°C. Membrane surface zeta potential, and thus estimation of membrane surface charge was calculated from the measured streaming potential. Dye solution concentration in feed and permeate was measured employing an ultraviolet-visible spectrophotometer (T80+ UV/VIS Spectrometer, PG Instruments) at the wavelength maximal absorption of the dye.

2.5. NF performance evaluation

A lab-scale cross-flow filtration setup was used to evaluate membrane permeation feature and dye removal efficiency. All the permeation test conditions were the same at a temperature of 25.0°C ± 1.0°C, pressure driving force of 6.0 bar, pH of approximately 7.0, and 40 L/h cross-flow velocity. In this circulation model, the retentate stream was circulated back to the feed tank by a pump with

Table 1
Types of membranes made by PVA and MOF particles and cross-linked by glutaraldehyde and sulfuric acid

Membrane label	% PVA concentration	MOF type	% MOF loading
P0.6	0.6%	–	–
P1	1%	–	–
P0.8	0.8%	–	–
P0.8-5	0.8%	NM101A	5%
P0.8-10	0.8%	NM101A	10%
P0.8-15	0.8%	NM101A	15%
P0.8-15-2	0.8%	NM101C	15%
P0.8-20	0.8%	NM101A	20%

open flow of 4 LPM and head of 130 psi. After measuring permeate volume and its solute content, it was returned to the feed tank to keep the feed concentration unchanged. The membranes sheets were placed in a Plexiglas cell with an effective filtration area of 29 cm^2 and compacted in 7.0 bar by de-ionized water before permeation tests to achieve a steady-state condition.

The pure water and dye solution permeability and rejection function of membranes were determined with de-ionized water and the aqueous solution of MB with dye concentrations of 10 mg/L. Also, the membrane performance in the separation of 500 ppm $AlCl_3$ polyvalent salt was evaluated.

First, pure water feed under 6.0 bar passed through the membrane surface, and pure water flux (J_{w0}) through the membrane was determined.

Filtration experiments were then carried out by 10 mg/L of dye solution as feed and checking the dye solution permeate flux (J_{wt}) for 30 min or until reaching steady-state flux (J_{ws}).

After dye solution filtration, membrane samples were flushed by de-ionized water under the cross-flow velocity of about 60 L/h for 0.5 h. Thus, loosely attached dye molecules were removed from the membrane surface, and then water permeate fluxes (J_{wc}) with de-ionized water were re-determined.

The following equation was used to determine the membrane permeate flux by using permeated water volume from a membrane with a specific effective area over a time interval [53].

$$J_w = \frac{V}{A \times \Delta T} \tag{2}$$

where J_w is the membrane permeate flux in L/m^2 h, A is the effective area of the membrane, and V is the volume of permeate over a specific period Δt.

The time-dependent flux for each tested membrane was used to investigate its fouling behaviors. Reversible and irreversible resistances of membranes were calculated using the following equations [53]:

$$R_r = \left(\frac{J_{wc} - J_{wt}}{J_{W0}}\right) \times 100 \tag{3}$$

$$R_{\text{ir}} = \left(\frac{J_{W0} - J_{wc}}{J_{W0}}\right) \times 100 \tag{4}$$

The following equations were used to determine relative flux reduction (RFR) and water recovery ratio (FRR), respectively [53]:

$$\text{RFR} = \left(1\frac{J_{wt}}{J_{w0}}\right) \times 100 \tag{5}$$

$$\text{FRR} = \left(\frac{J_{wc}}{J_{w0}}\right) \times 100 \tag{6}$$

As mentioned above, J_{w0}, J_{ws}, and J_{wc} are pure water, filtrated, and water-cleaned membranes permeate flux, respectively.

High FRR value indicates that the cleaning efficiency is acceptable and low values of RFR and membrane resistances means better antifouling properties. The dye rejection (R) is determined using the following equation [53]:

$$R = \left(1 - \frac{C_p}{C_f}\right) \times 100 \tag{7}$$

in which C_f and C_p are the dye concentrations in feed tank and permeate collection reservoir, respectively. Also, by measuring the conductivity of the $AlCl_3$-containing solution using a conductivity meter, the amount of $AlCl_3$ concentration was obtained.

3. Results and discussion

3.1. Characterization of MOFs and MOF loaded membranes

The crystallinity of NM101A and NM101C were monitored by XRD. Based on Fig. 1, XRD patterns of the synthesized NM101A and NM101C showed clearly separate peaks at angles (2θ) of 8.87°, 16.8°, and 25.5° and indicated the same structural characteristic in consistent with the reported works [42,54].

FTIR patterns of the MOFs are demonstrated clearly in Fig. 2. NM101A, the first characteristic peak at 3,892.08 cm^{-1} belonged to the Al–OH groups, whereas NM101C, Cr–OH vibration was moved a little (3,917 cm^{-1}). Asymmetrical stretching of the amino groups ($-NH_2$) at 3,469.7 cm^{-1} and their symmetrical stretching at 3,546.85 cm^{-1} indicated that in both MOFs structures, they were free for interaction [55]. These absorptions were formed by the contribution of two different bands indicating two amine species in the framework. Additionally, the appearance of bands at 3,203.54 and 3,053.10 cm^{-1} suggests the interaction between the amines with the framework or with each other [56]. In this regard, two characteristic peaks at 1,622.02 and 1,257.50 cm^{-1} [43] denote the N–H bending vibration and C–N stretching vibration of aromatic amines in the lower frequency region, respectively. The amine group can lead to positive membrane charge.

Fig. 3 shows the surface (left) and cross-section (right) FESEM images of the membranes. According to cross-section FESEM (Fig. 3a), a polysulfone membrane with a thickness of about 75 microns had an asymmetric morphology with a thin upper layer, small cavities, high porosity, and a bottom layer with finger-like holes. By comparing FESEM images of polysulfone substrate and PVA coated membrane (Fig. 3a and b), it was found that the membrane surface became denser following PVA coating. This dense layer was attributed to the PVA skin layer on top of the polysulfone membrane surface. According to the cross-section FESEM images and IDFIX Report (Fig. 4), the PVA skin layer thickness was about 800 nm. This hydrophilic layer enhanced the membrane permeate flux by reducing transmembrane resistance. FESEM images of the synthesized NM101A and NM101C in the membrane

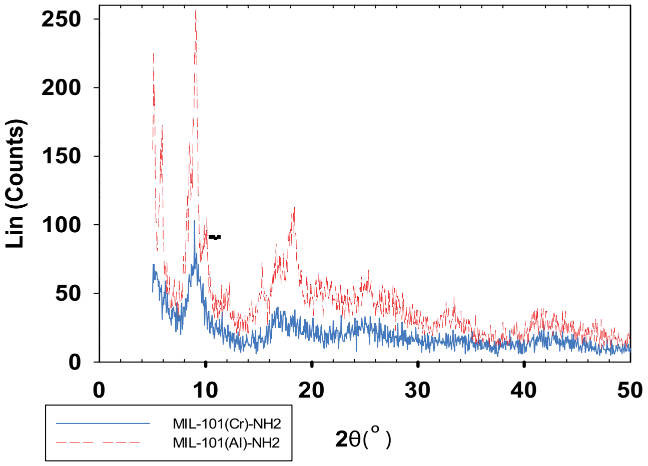

Fig. 1. XRD patterns of NM101A and NM101C.

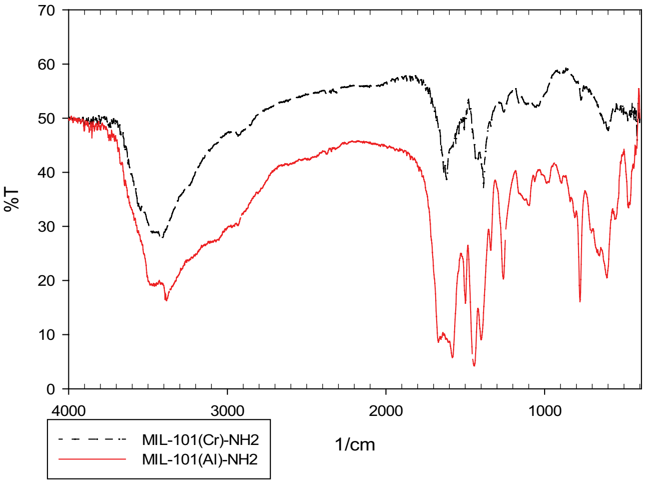

Fig. 2. FTIR results of NM101A and NM101C.

matrix (Fig. 3c and d) show that the NM101A particles were smaller and more aggregate than the NM101C crystals. Thus, the P0.8-15 membrane skin layer with NM101A filler was slightly thinner than the P0.8-15-2 membrane containing NM101C filler. Also, MOF particles were well dispersed in the PVA dense layer. The widespread presence of MOF particles on the membrane surface makes them more accessible to the feed solution and can increase dye rejection and improve fouling resistance.

3.2. Zeta potential and membranes surface charge

Zeta potential results are revealed in Table 2. "Zeta potential values" at pH = 7.0 indicated that the membranes have more positive charge by adding both NM101A and NM101C particles and neutralizing the effect of amphiphilic substances. These findings are supported by results from a previous study performed on adsorption of MB and MO by NH_2-MIL-101 [57]. This positive charge can be increased by elevating MOF loadings. The same upward trend has been observed in other works [55]. This phenomenon is because of the presence of MOFs in membranes surface that have positive charge amine groups. In addition, at 15% MOF loading, the NM101A/PVA membrane (P0.8-15) zeta potential were slightly higher than those of NM101C/PVA membrane (P0.8-15-2). The molecular weight of NM101A (223 Da) is lower than NM101C (248 Da), so at equal weight percentages, the molar content for the NM101A is higher than NM101C. Higher positive charge of the NM101A loaded membrane surface than that of NM101C can be due to the molar content difference.

3.3. Water contact angle results and hydrophilicity of membranes

The water contact angle of support and modified membranes are listed in Table 3. According to the measured values, the membranes hydrophilicity was significantly increased by coating the PVA polymer on the polysulfone substrate, that is, adding fillers in PVA matrix reduces the effect of the hydrophilicity. However, in large amounts of NM101A, the water contact angle was reduced. High concentration of MOFs, surface roughness, high aggregation of hydrophilic free amine groups, or gaps between PVA and MOFs can reduce the water contact angle. At the same MOF loading, the membrane filled with NM101A had a smaller contact angle and more hydrophilicity than NM101C.

3.4. Selecting the optimal concentration of PVA as the coating polymer

According to Fig. 5, comparison of different PVA concentrations to cover the polysulfone membrane surface showed that by increasing the PVA concentration from 0.6 to 0.8 wt.%, the pure water flux and the dye solution permeate flux were decreased slightly. This reduction was sharper for 1 wt.% of PVA. Furthermore, the MB rejection was increased with increasing PVA concentration and membrane coating layer thickness. Thus, a thicker PVA dense layer increased the membrane resistance against water passage and rejected more dye molecules. In the following, a concentration of 0.8 wt.% PVA was selected as the coating layer matrix.

3.5. Comparison the effect of two types of MOFs NM101A and NM101C on the performance of NF membrane

Dye separation performance of two NF membrane types incorporating NM101A and NM101C as filler with the identical MOF content of 15% are compared in Fig. 6. It was evident that in the same condition, permeation and dye rejection for membrane with NM101A as filler was almost higher than that of NM101C, while both rejection and permeate for PVA modified membrane without MOF were the least of all. NM101A particles had a polyhedral morphology with a smaller diameter than NM101C with grainy particles. So, according to cross-section FESEM figures (Fig. 3), the skin layer thickness for NM101A/PVA membrane was slightly thinner than NM101C/PVA membrane, and this could be the cause of its higher permeate flux.

The contact angle results showed that hydrophilicity of NM101A/PVA membrane was slightly higher than

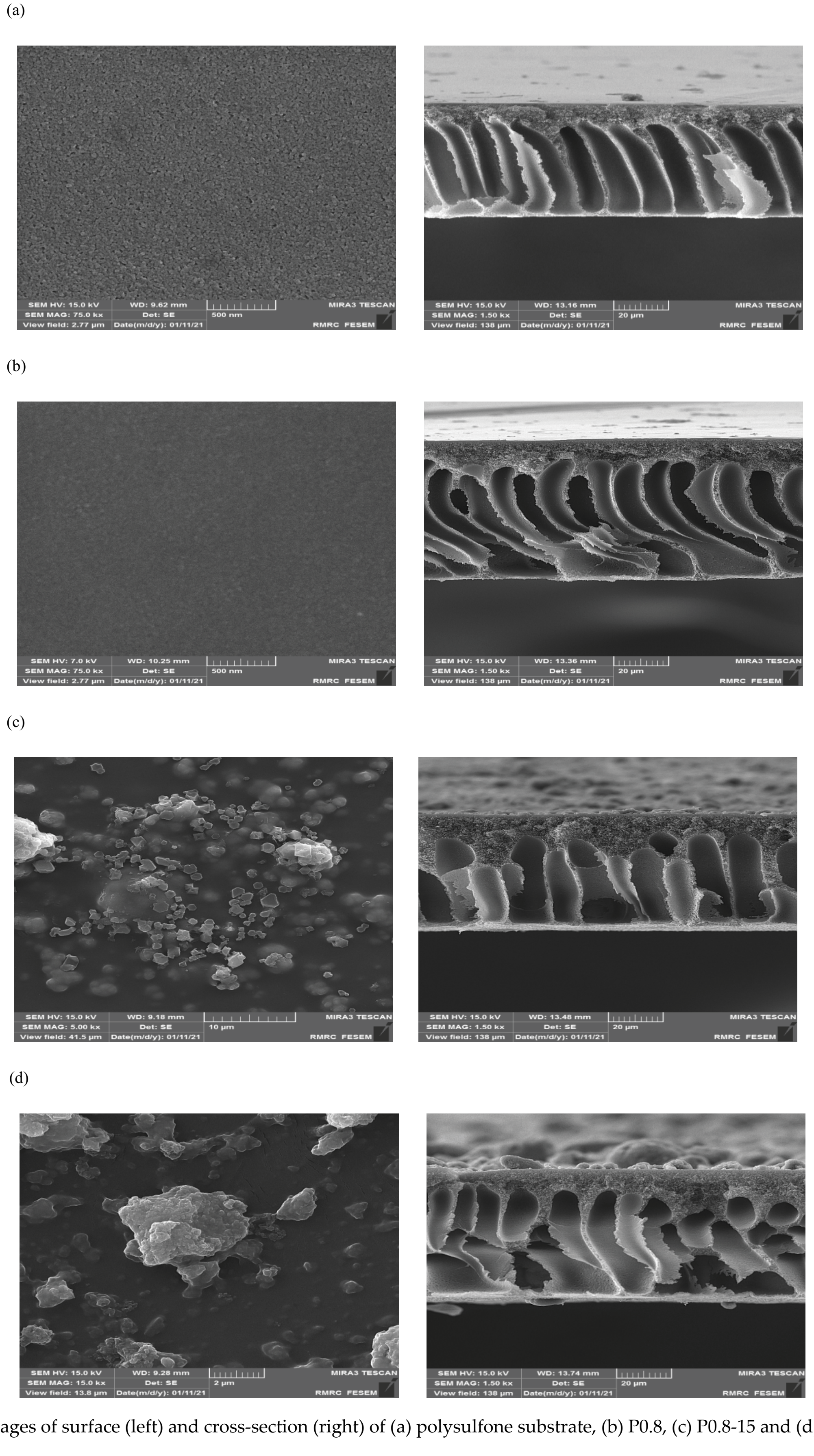

Fig. 3. FESEM images of surface (left) and cross-section (right) of (a) polysulfone substrate, (b) P0.8, (c) P0.8-15 and (d) P0.8-15-2.

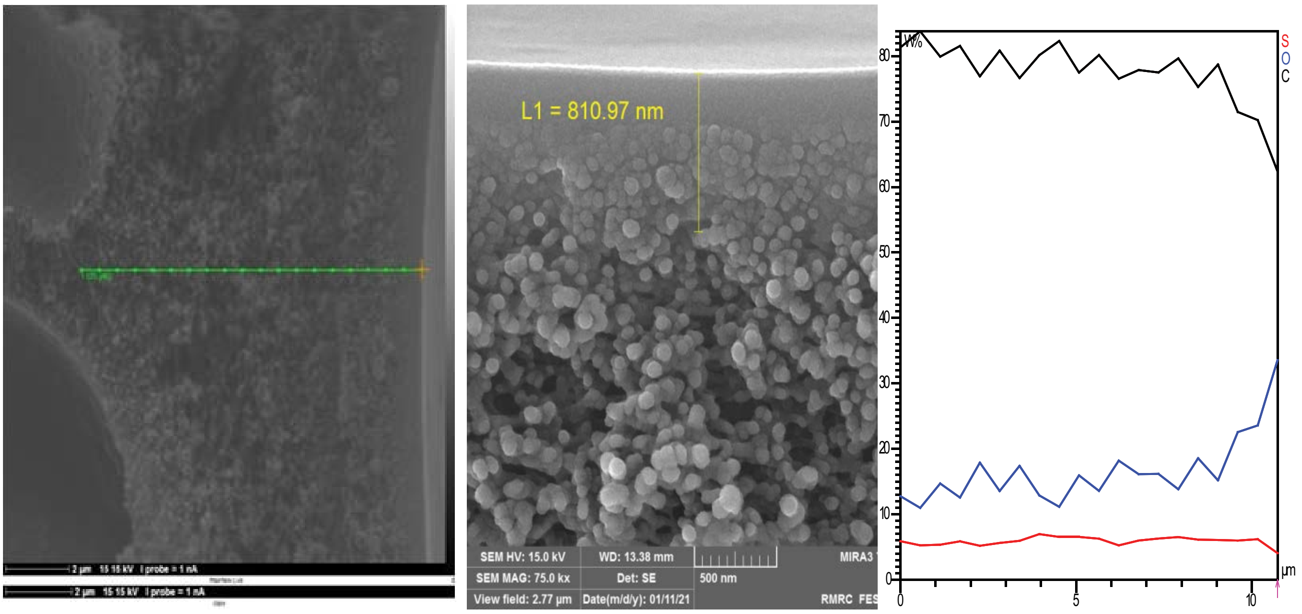

Fig. 4. IDFIX Report of P0.8 membrane.

Table 2
Zeta potential values of different membranes

Membrane type	Filler type	Zeta potential value (mV) at pH 7.0
P0.8	–	11.72
P0.8-15	NM101A	16.168
P0.8-15-2	NM101C	15.30

Table 3
Water contact angle values of different membranes

Membrane type	Membrane contact angle (°)
Support membrane	74.38
P0.8	36.78
P0.8-5	38.55
P0.8-10	47.46
P0.8-15	37.28
P0.8-15-2	39.41
P0.8-20	28.62

NM101C/PVA membrane. This higher hydrophilicity can cause higher water permeation and dilute the dye concentration in permeate and increase the rejection [58]. That is to say, a more positive charge for the NM101A/PVA membrane increased the cationic dye rejection and increased water permeate by decreasing fouling. According to the results, it was concluded that NM101A can be used as a filler in the PVA matrix.

Some parameters were calculated by pure water flux and dye solution permeate flux according to Eqs. (3)–(6). The results are compared in Fig. 7 for membranes made with two types of MOFs. Reversible and irreversible resistances for the P0.8-15 membrane, as well as RFR, were slightly lower than the P0.8-15-2 membrane, and this feature can be due to more surface positive charge, more hydrophilicity and less skin layer thickness of P0.8-15 membrane. These factors caused higher rejection and permeate flux of the P0.8-15 membrane. The flux return ratio for the P0.8-15 was also higher than P0.8-15-2.

3.6. Investigating the effect of different percentages of filler in the PVA matrix on dye separation performance

The effect of MOF contents, including 0% to 20% of NM101A, on the permeate flux and rejection was investigated. For a more detailed characterization of membrane morphology, FESEM images proved to be helpful. Fig. 8 shows the results of membrane permeability and dye rejection for all NM101A/PVA membranes with different amounts of NM101A loadings (0%, 5%, 10%, 15%, and 20%).

Pure water flux was decreased with MOF loading. This effect can be due to the increase in density and concentration of the coating solution and cross-linking between the amine groups at NM101A and hydroxyl groups of PVA in membrane surface. In fact, porosity and some properties of MOF particles within the PVA matrix had a positive effect on increasing the pure water flux. These properties created additional pathways for water to pass through the membrane, but its impact on increasing pure water flux was negligible.

In the dye solution filtration section, with the addition of MOF particles as filler up to 10%, the average amount of dye solution permeates increased, then it decreased very slightly to 15%, and finally reduced sharply to 20%. Some factors, such as the concentration and the skin layer thickness, cross-linking between membranes components, MOFs porosity and additional paths for water,

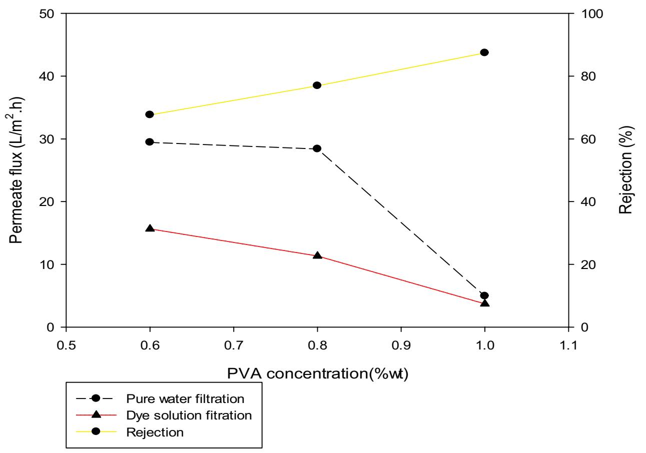

Fig. 5. Performance of membranes with different PVA concentrations (wt.%).

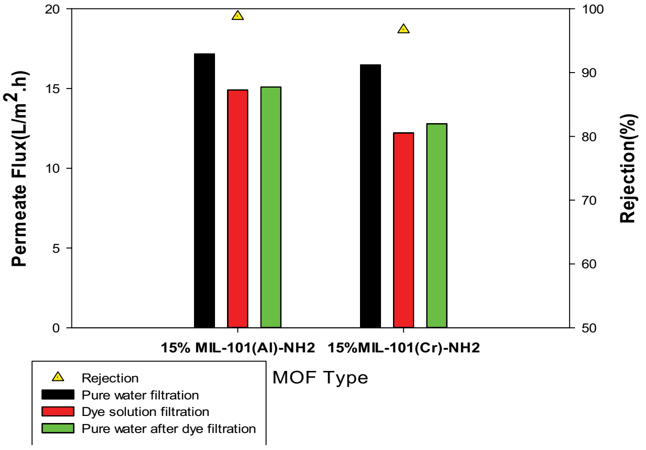

Fig. 6. Performance of different membranes containing 15% of NM101A and NM101C.

hydrophilicity, surface charge and thus the higher rejection of dye particles, and low fouling could explain this trend of flux changes.

At first, because of the electrostatic repulsion and improvement of 'dye' rejection and membrane fouling, the dye solution permeate flux increased. Gradually, with the MOF ratio rising, a decreasing trend was seen in the permeate flux, due to the dominance of concentration and thickness of the skin layer. For PM0.8-20 with 20% MOF loading, the negative effect of the coating solution concentration on membrane permeability was very high, and the amount of permeate flux was not acceptable.

The upward trend of dye rejection was also maintained by placing more MOF particles in the PVA matrix. When the coating solution was concentrated, the membrane skin layer became thicker and more compact with a smaller pore size that prevented the passage of dye molecules. That is to say, in higher MOF-loaded membranes with greater charge density were rejected positively charged amine functional groups more cations. Since in high quantities of MOF loadings (up to 20%), dye rejection had an upward trend, so the possibility of gaps in membrane surface at these amounts was discarded. It was clear that the P0.8-10 with 10% MOF loading had the highest permeability (approximate 15.03 L/m^2 h) while P0.8-20 with 20% MOF loadings had the highest rejection (99.18%) and P0.8-15 with a good permeability and rejection (14.91 L/m^2 h and 98.8% respectively) has been the best choice. This membrane (P0.8-15) rejected 14% of $AlCl_3$ polyvalent ion from water.

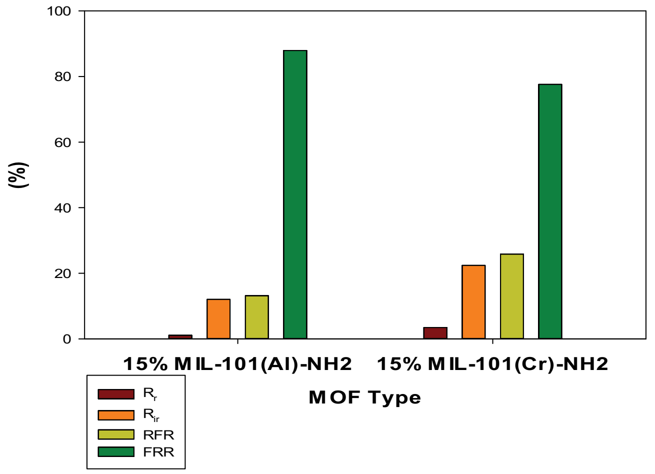

Fig. 7. Comparison of resistances, RFR and FRR for membranes containing 15% of NM101A with NM101C.

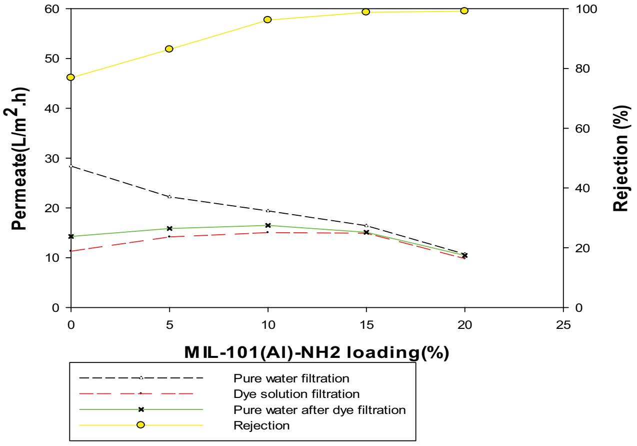

Fig. 8. Performance of membranes with different NM101A loading.

Also Fig. 9 shows the trend of some parameters such as R_r, R_{ir}, RFR, and FRR vs. NM101A content. Adding more MOF particles into the PVA matrix reduced the membrane fouling and increased the parameter of flux return ratio due to the improved properties of surface and membrane performance. The noteworthy point is that the performance of membranes has been investigated for a limited time. Considering the results of irreversible resistance and membrane flux return ratio, the membranes with higher MOF percentage was expected to have a higher stable flux over a more extended time.

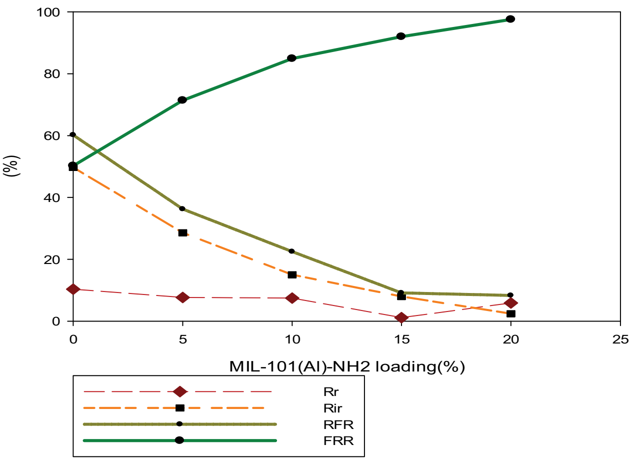

Fig. 9. Resistances, RFR and FRR for membranes with different NM101A loading.

The results of flux, rejection and fouling parameters related to this membrane were competitive with the values of other studies as well as membranes used in industry and can separate a large part of dyes and solutes from colored effluents [59,60].

4. Conclusion

NM101A and NM101C were utilized as fillers in PVA polymeric matrix to fabricate a novel NF membrane. The presence of amine groups and consequently positive charge in these MOFs helped enhance the molecule repulsion of cationic dye. FESEM characterization revealed that particles of MOF were equally located on the membrane surface within the PVA matrix. The NM101A particles formed a thinner layer on the polysulfone substrate due to their smaller size compared to NM101C. As a rule, this layer becomes thicker by adding more MOF particles. Zeta potential results also showed that the surface of the membrane filled with NM101A had a more positive charge, and this positive charge was increased at high MOF loadings. By comparing membranes fabricated with two types of MOFs with the same load, it was observed that the membrane containing NM101A had higher permeability and also rejected more cationic dye molecules. Among the membranes with different MOF loadings, the best permeate flux was related to P0.8-10, and the best rejection was related to P0.8-20, but the P0.8-15 membrane had both high permeate flux and rejection. This membrane has shown at least 14% rejection in the separation of $AlCl_3$ polyvalent ions.

References

[1] M.M. Hassan, C.M. Carr, A critical review on recent advancements of the removal of reactive dyes from dyehouse effluent by ion-exchange adsorbents, Chemosphere, 209 (2018) 201–219.

[2] S. Radoor, J. Karayil, J. Parameswaranpillai, S. Siengchin, Adsorption of methylene blue dye from aqueous solution by a novel PVA/CMC/halloysite nanoclay bio composite: characterization, kinetics, isotherm and antibacterial properties, J. Environ. Health Sci. Eng., 18 (2020) 1311–1327.

[3] F. Mashkoor, A. Nasar, Magsorbents: potential candidates in wastewater treatment technology – a review on the removal of methylene blue dye, J. Magn. Magn. Mater., 500 (2020) 166408, doi: 10.1016/j.jmmm.2020.166408.

[4] P. Borthakur, M.R. Das, Hydrothermal assisted decoration of NiS_2 and CoS nanoparticles on the reduced graphene oxide nanosheets for sunlight driven photocatalytic degradation of azo dye: effect of background electrolyte and surface charge, J. Colloid Interface Sci., 516 (2018) 342–354.

[5] C.I. Ezugwu, M.A. Asraf, X. Li, S. Liu, C.M. Kao, S. Zhuiykov, F. Verpoort, Selective and adsorptive removal of anionic dyes and CO_2 with azolium-based metal–organic frameworks, J. Colloid Interface Sci., 519 (2018) 214–223.

[6] S. Yang, C.Y. Xu, B.Y. Zhang, L. Yang, S.P. Hu, L. Zhen, Ca(II) doped beta-In_2S_3 hierarchical structures for photocatalytic hydrogen generation and organic dye degradation under visible light irradiation, J. Colloid Interface Sci., 491 (2017) 230–237.

[7] A. Habibi, Z. Mehrabi, Aerobic degradation of methylene blue from colored effluents by *Ralstonia eutropha*, Pollution, 3 (2017) 363–375.

[8] W. Qian, T. Senlin, N. Ping, Degradation mechanism of methylene blue in a heterogeneous Fenton-like reaction catalyzed by ferrocene, Ind. Eng. Chem. Res., 53 (2014) 643–649.

[9] M.I. Arun, S.S. Seema, A.F. Ismail, J.S. Simon, Al-A. Amir, Humic acid based biopolymeric membrane for effective removal of methylene blue and rhodamine B, Ind. Eng. Chem. Res., 54 (2015) 4965–4975.

[10] J.R. Werber, C.O. Osuji, M. Elimelech, Materials for next-generation desalination and water purification membranes, Nat. Rev. Mater., 1 (2016) 16018, doi: 10.1038/natrevmats.2016.18.

[11] J.E. Gu, S. Lee, C.M. Stafford, J.S. Lee, W. Choi, B.-Y. Kim, K.-Y. Baek, E.P. Chan, J.Y. Chung, J. Bang, J.-H. Lee, Molecular layer-by-layer assembled thin-film composite membranes for water desalination, Adv. Mater., 25 (2013) 4778–4782.

[12] M. Elimelech, W.A. Phillip, The future of seawater desalination: energy, technology, and the environment, Science, 333 (2011) 712–717.

[13] Y. Zhong, S. Mahmud, Z. He, Y. Yang, Z. Zhang, F. Guo, Z. Chen, Z. Xiong, Y. Zhao, Graphene oxide modified membrane for highly efficient wastewater treatment by dynamic combination of nanofiltration and catalysis, J. Hazard. Mater., 397 (2020) 122774, doi: 10.1016/j.jhazmat.2020.122774.

[14] Q. Qian, W.S. Chi, G. Han, Z.P. Smith, Impact of post synthetic modification routes on filler structure and performance in metal–organic framework-based mixed-matrix membranes, Ind. Eng. Chem. Res., 59 (2020) 5432–5438.

[15] Y.-L. Ji, W.-J. Qian, Y.-W. Yu, Q.-F. An, L.-F. Liu, Y. Zhou, C.-J. Gao, Recent developments in nanofiltration membranes based on nanomaterials, Chin. J. Chem. Eng., 25 (2017) 1639–1652.

[16] S. Jeffery-Black, S.J. Duranceau, The influence of solute polarizability and molecular volume on the rejection of trace organics in loose nanofiltration membrane processes, Desal. Water Treat., 57 (2016) 29059–29069.

[17] M.F. Jimenez-Solomon, Q. Song, K.E. Jelfs, M. Munoz-Ibanez, A.G. Livingston, Polymer nanofilms with enhanced microporosity by interfacial polymerization, Nat. Mater., 15 (2016) 760–767.

[18] S. Liu, M. Zhang, F. Fang, L. Cui, J. Wu, R. Field, K. Zhang, Biogenic silver nanocomposite TFC nanofiltration membrane with antifouling properties, Desal. Water Treat., 57 (2016) 10560–10571.

[19] S. Jalali, A.R. Mehrabadi, J. Shayegan, M. Mirabi, S.S. Madaeni, Flux enhancement of thin-film composite membrane by graphene oxide incorporation, J. Environ. Health Sci. Eng., 17 (2019) 377–382.

[20] L. Yang, W. Zhenyi, F. Wangxi, Z. Yuzhang, Z. Yatao, J. Jian, Polyamide thin films grown on PD/SWCNT-interlayered-PTFE microfiltration membranes for high-permeance organic solvent nanofiltration, Ind. Eng. Chem. Res., 59 (2020) 22533–22540.

[21] W. Zhenyi, W. Zhangxin, L. Shihong, J. Huile, G. Shoujian, Z. Yuzhang, J. Jian, Nanoparticle-templated nanofiltration membranes for ultrahigh performance desalination, Nat. Commun., 9 (2018) 2004, doi: 10.1038/s41467-018-04467-3.

[22] A.A. Sapalidis, Porous polyvinyl alcohol membranes: preparation methods and applications, Symmetry, 12 (2020) 960, doi: 10.3390/sym12060960.

[23] G. Yang, Z. Xie, C.M. Doherty, M. Cran, D. Ng, S. Gray, Understanding the transport enhancement of poly(vinyl alcohol) based hybrid membranes with dispersed nanochannels for pervaporation application, J. Membr. Sci., 603 (2020) 118005, doi: 10.1016/j.memsci.2020.118005.

[24] M.G. Katz, T. Wydeven, in: Synthetic Membranes, A.F. Turbak, Ed., ACS Symposium Series 153, American Chemical Society, Washington, D.C., 1981, pp 383–398.

[25] B. Bolto, T. Tran, M. Hoang, Z. Xie, Cross-linked poly(vinyl alcohol) membranes, Prog. Polym. Sci., 34 (2009) 969–981.

[26] H. Dong, L. Zhao, L. Zhang, H. Chen, C. Gao, W.S. Winston Ho, High-flux reverse osmosis membranes incorporate with NaY zeolite nanoparticles for brackish water desalination, J. Membr. Sci., 476 (2015) 373–383.

[27] M. Kadhom, J. Yin, B. Deng, A thin film nanocomposite membrane with MCM-41 silica nanoparticles for brackish water purification, Membranes, 6 (2016) 1–12.

[28] J.-T. Jung, W.-H. Lee, J.-O. Kim, Photodegradation and permeability of conventional photocatalytic reactor and two different submerged membrane photocatalytic reactors for the removal of humic acid in water, Desal. Water Treat., 57 (2016) 26765–26772.

[29] W. Li, Y. Zhang, Q. Li, G. Zhang, Metal–organic framework composite membranes: synthesis and separation applications, Chem. Eng. Sci., 135 (2015) 232–257.

[30] G.-R. Xu, Z.-H. An, K. Xu, Q. Liu, R. Das, H.-L. Zhao, Metal–organic framework (MOF)-based micro/nanoscaled materials for heavy metal ions removal: the cutting-edge study on designs, synthesis, and applications, Coord. Chem. Rev., 427 (2021) 213554, doi: 10.1016/j.ccr.2020.213554.

[31] X. Zhang, R.-B. Lin, J. Wang, B. Wang, B. Liang, T. Yildirim, J. Zhang, W. Zhou, B. Chen, Optimization of the pore structures of MOFs for record high hydrogen volumetric working capacity, Adv. Mater., 32 (2020) 1907995, doi: 10.1002/adma.201907995.

[32] Sh. Xiao, X. Huo, Sh. Fan, K. Zhao, Sh. Yu, X. Tan, Design and synthesis of Al-MOF/PPSU mixed matrix membrane with pollution resistance, Chin. J. Chem. Eng., 29 (2021) 110–120.

[33] G. Gnanasekaran, G. Arthanareeswaran, Y.S. Mok, A high-flux metal–organic framework membrane (PSF/MIL-100 (Fe)) for the removal of microplastics adsorbing dye contaminants from textile wastewater, Sep. Purif. Technol., 277 (2021) 119655, doi: 10.1016/j.seppur.2021.119655.

[34] K. Shen, L. Zhang, X. Chen, L. Liu, D. Zhang, Y. Han, J. Chen, J. Long, R. Luque, Y. Li, B. Chen, Ordered macro microporous metal–organic framework single crystals, Science, 359 (2018) 206–210.

[35] F. Aghili, A. Ghoreyshi, A. Rahimpour, B. Van der Bruggen, New chemistry for mixed matrix membranes: growth of continuous multilayer UiO-66-NH_2 on UiO-66-NH_2-based polyacrylonitrile for efficient separation, Ind. Eng. Chem. Res., 59 (2020) 7825–7838.

[36] H. Sun, B. Tang, P. Wu, Hydrophilic hollow zeolitic imidazolate framework-8 modified ultrafiltration membranes with significantly enhanced water separation properties, J. Membr. Sci., 551 (2018) 283–293.

[37] G. Gnanasekaran, S. Balaguru, G. Arthanareeswaran, D.B. Das, Removal of hazardous material from wastewater by using metal–organic framework (MOF) embedded polymeric membranes, Sep. Sci. Technol., 54 (2018) 434–446.

[38] S. Sorribas, P. Gorgojo, C. Téllez, J. Coronas, A.G. Livingston, High flux thin film nanocomposite membranes based on metal–organic frameworks for organic solvent nanofiltration, J. Am. Chem. Soc., 135 (2013) 15201–15208.

[39] S. Surble, F. Millange, C. Serre, G. Férey, R.I. Walton, An EXAFS study of the formation of a nanoporous metal–organic framework: evidence for the retention of secondary building units during synthesis, Chem. Commun., 14 (2006) 1518–1520.

[40] C. Serre, F. Millange, S. Surble, G. Férey, A route to the synthesis of trivalent transition-metal porous carboxylates with trimeric secondary building units, Angew. Chem. Int. Ed., 43 (2004) 6285–6289.

[41] J. Ma, Y. Ying, X. Guo, H. Huang, D. Liu, C. Zhong, Fabrication of mixed-matrix membrane containing metal–organic framework composite with task-specific ionic liquid for efficient CO_2 separation, J. Mater. Chem., 4 (2016) 7281–7288.

[42] A. Nuhnen, M. Klopotowski, H.B. Tanh Jeazet, S. Sorribas, B. Zornoza, C. Téllez, J. Coronas, C. Janiak, High performance MIL-101(Cr)@6FDA-mPD and MOF-199@6FDA-mPD mixed-matrix membranes for CO_2/CH_4 separation, Dalton Trans., 49 (2020) 1822–1829.

[43] M. Babar, M. Mubashir, A. Mukhtar, S. Saqib, S. Ullah, M.A. Bustam, P.L. Show, Sustainable functionalized metal–organic framework NH_2-MIL-101(Al) for CO_2 separation under cryogenic conditions, Environ. Pollut., 279 (2021) 116924, doi: 10.1016/j.envpol.2021.116924.

[44] R. Lin, L. Ge, S. Liu, V. Rudolph, Z. Zhu, Mixed-matrix membranes with metal–organic framework-decorated CNT fillers for efficient CO_2 separation, ACS Appl. Mater. Interfaces, 7 (2015) 14750–14757.

[45] X. Li, Y. Pi, Q. Xia, Z. Li, J. Xiao, TiO_2 encapsulated in salicylaldehyde-NH_2-MIL-101(Cr) for enhanced visible light-driven photodegradation of MB, Appl. Catal., B, 191 (2016) 192–201.

[46] K. Leus, T. Bogaerts, J. De Decker, H. Depauw, K. Hendrickx, H. Vrielinck, V. Van Speybroeck, P. Van Der Voort, Systematic study of the chemical and hydrothermal stability of selected "stable" metal–organic frameworks, Microporous Mesoporous Mater., 226 (2016) 110–116.

[47] I. Simonsson, Ph. Gärdhagen, M. Andrén, P.L. Tam, Z. Abbas, Experimental investigations into the irregular synthesis of iron(III) terephthalate metal–organic frameworks MOF-235 and MIL-101, Dalton Trans., 50 (2021) 4976–4985.

[48] S. Cohen, M. Post-synthetic methods for the functionalization of metal–organic frameworks, Chem. Rev., 112 (2012) 970–1000.

[49] A.D. Burrows, Mixed-component metal–organic frameworks (MC-MOFs): enhancing functionality through solid solution formation and surface modifications, Cryst. Eng. Commun., 13 (2011) 3623–3642.

[50] R. Bibi, L. Wei, Q. Shen, W. Tian, O. Oderinde, N. Li, J. Zhou, Effect of amino functionality on the uptake of cationic dye by titanium-based metal–organic frameworks, J. Chem. Eng. Data, 62 (2017) 1615–1622.

[51] E.V. Ramos-Fernandez, C. Pieters, B. van der Linden, J. Juan-Alcañiz, P. Serra-Crespo, M.W.G.M. Verhoeven, H. Niemantsverdriet, J. Gascon, F. Kapteijn, Highly dispersed platinum in metal–organic framework NH_2-MIL-101(Al) containing phosphotungstic acid – characterization and catalytic performance, J. Catal., 289 (2012) 42–52.

[52] D. Jiang, L.L. Keenan, A.D. Burrows, K.J. Edler, Synthesis and post-synthetic modification of MIL-101(Cr)-NH_2 via a tandem diazotisation process, Chem. Commun., 48 (2012) 12053–12055.

[53] T.Ch. Ying, E. Mahmoudi, A.W. Mohammad, A. Benamor, D. Johnson, N. Hilal, Development of polysulfone-nanohybrid membranes using ZnO-GO composite for enhanced antifouling and antibacterial control, Desalination, 402 (2017) 123–132.

[54] Z.-Q. Bai, L.-Y. Yuan, L. Zhu, Z.-R. Liu, S.-Q. Chu, L.-R. Zheng, J. Zhang, Z.-F. Chai, W.-Q. Shi, Introduction of amino groups into acid-resistant MOFs for enhanced U(VI) sorption, J. Mater. Chem., 3 (2015) 525–534.

[55] X.-H. Ma, Z. Yang, Z.-K. Yao, Z.-L. Xu, C.Y. Tang, A facile preparation of novel positively charged MOF/chitosan nanofiltration membranes, J. Membr. Sci., 525 (2017) 269–276.

[56] P. Serra-Crespo, E.V. Ramos-Fernandez, J. Gascon, F. Kapteijn, Synthesis and characterization of an amino functionalized MIL-101(Al): separation and catalytic properties, Chem. Mater., 23 (2011) 2565–2572.

[57] X. Zhao, M. Zheng, X. Gao, Zh. Gao, H. Huang, Construction of an anionic porous framework via a post-synthesis strategy to

regulate the adsorption behavior of organic pollutants, J. Mater. Sci., 55 (2020) 14751–14760.

[58] A.G. Fane, C.Y. Tang, R. Wang, Membrane Technology for Water: Microfiltration, Ultrafiltration, Nanofiltration, and Reverse Osmosis, A2 – Wilderer, Peter, Treatise on Water Science, Elsevier, Oxford, 2011, pp. 301–335.

[59] A.E. Abdelhamid, A.A. El-Sayed, A.M. Khalil, Polysulfone nanofiltration membranes enriched with functionalized graphene oxide for dye removal from wastewater, J. Polym. Eng., 40 (2020) 833–841.

[60] R. Zhang, Y. Liu, Y. Li, Q. Han, T. Zhang, K. Zeng, Ch. Zhao, Polyvinylidene fluoride membrane modified by tea polyphenol for dye removal, J. Mater. Sci., 55 (2020) 389–403.